Geologic Signatures of Atmospheric Effects on Impact Cratering on Venus

Final Technical Report NAGW-3431

The proposal "Geologic Signatures of Atmospheric Effects on Impact Cratering on Venus" was submitted to the Venus Data Analysis Program as a three year proposal. Due to budgetary reductions at Headquarters, this program was reduced to an 18 month program, thereby affecting the overall scope of the proposed research. The proposed effort originally focused on three objectives: 1) to contrast the response of the surface (cratering) and atmosphere (blast effects) to bolides with respect to scale, intensity, and time. 2) To characterize the energy, momentum, and nature of impactors following crater formation; and 3) To assess energy scaling relations for impact craters on Venus from source energies inferred from contrasting surface expressions of atmospheric effects and crater size. The strategy for the proposed research included: laboratory experiments at the NASA Ames Vertical Gun Range in order to assess the effect of an atmosphere on blast generation and entry physics; geologic studies of surface features on Venus as signatures of blast effects and energy coupling as a function of impact angle; and to document the time evolving winds created in response to crater formation.

The reduced scope of the VDAP seriously affected completion of projects originally intended as a longer term effort. Nevertheless, considerable progress was made that provided seeds for projects eventually absorbed in ongoing efforts of other continuing NASA grants. The following list highlights accomplishments over the award period:

1) Geologic Signatures of Impact Energy

   a) Laboratory experiments were performed using the NASA Ames Vertical Gun Range (AVGR) to assess the interaction between disrupted impactor and atmosphere during entry. These experiments used Schlieren imaging and witness plates to determine the process controlling dispersal of impactor fragments. In contrast with expectations (Melosh, 1981), these experiments demonstrated that the pressure jump across the mach boundary acts to

restrict the outward expansion of debris, thereby resulting in collimation rather than dispersal of a debris cloud as it passes through an atmosphere. A theoretical model was developed to allow extrapolating the laboratory results to conditions on Venus in order to understand the creation of distinctive blast haloes on its surface. The results were presented at the Lunar and Planetary Science Conference (Schultz and Sugita, 1994).

b) Laboratory experiments at the AVGR also were performed to assess the energy coupling between impacts and the surrounding atmosphere. These studies were intended to address the energy-coupling efficiency to the atmosphere and the evolution of the surface blast. The results of this study were folded into other efforts after the termination of VDAP.

2) Atmospheric Response to Crater Formation

a) During the grant period, the evolution of the impactor following impact was studies using Schlieren imaging at the AVGR, Magellan imaging, and theoretical studies. Schlieren imaging documented the downrange blast front created by vaporization during oblique impacts. This provided a basis for fluid dynamical calculations describing containment and deceleration of a downrange-moving and expanding vapor cloud under conditions on Venus (Sugita and Schultz, 1994, 1995). The calculations showed that the ratio of the distance of run-out flows to the zone of interference with downrange ejecta emplacement increases as impact angle decreases, consistent with observations of craters on Venus. An important result of these calculations is that aerodynamic reshaping of the vapor cloud may be required to explain differences between observations and calculations.

b) Laboratory experiments allowed assessing the effect of impact angle on coupling efficiency with an atmosphere. These results contributed to a paper of broader scope dealing with impact vaporization (Schultz, 1996).

c) Recognizing the effect of impact angle on surface blasts and run-out flows allowed distinguishing between crater clusters created by simultaneous impacts and clusters created by isolated regions of older age. This strategy revealed "islands" of ancient terrains on Venus previously dismissed as statistical clumping. Poisson statistics and comparisons with lunar crater statistics are consistent with the finding (Schultz, 1993, 1994).

Published Abstracts and Papers Resulting from VDAP Support

1) Schultz, P.H., 1993a, Visualizing the Nature and Consequences of the Chicxulub Impactor: Clues from Venus, *LPI Contrib. 825*, 104-105.
2) Schultz, P.H., 1993b, Searching for Ancient Venus, *Lunar and Planet. Sci. XXIV*, 1255-1256.
3) Schultz, P.H., 1994, Islands in Time on Venus, *Eos 75*, 214-215.
4) Schultz, P.H. and Sugita, S., 1994, Penetrating and Escaping the Atmospheres of Venus and the Earth, *Lunar and Planet. Sci. XXV*, 1215-1216.
5) Sugita, S. and Schultz, P.H., 1994, Impact Ejecta Vapor Cloud Interference Around Venus Craters, *Lunar and Planet. Sci. XXV*, 1355-1356.
6) Schultz, P.H. and Sugita, S., 1995, Dynamical Evolution of Vapor Clouds by Oblique Impacts on Venus, *Lunar and Planet. Sci. XXVI*, 1369-1370.
7) Schultz, P.H., 1996, Effect of Impact Angle on Vaporization, *J. Geophys. Res.* (in review).
8) Sugita, S. and Schultz, P. H., 1996, Impact Vapor Generation Inferred from Run-out Flows on Venus, *Lunar and Planet. Sci. XXVII* (in press).

Searching for Ancient Venus.

Peter H. Schultz, Department of Geological Sciences, Brown University, Providence, RI 02912.

The cratering record on Venus provides one of the few available remote chronometers for establishing relative age. Because the dense atmosphere shields the surface from smaller impactors, the most statistically significant fraction of the cratering record is incomplete at best and indeterminate at worst. Larger craters represent survivors of entry but occur too infrequently for delineating statistically significant ages on a local scale (1). This contribution reconsiders processes affecting the statistical cratering record and argues that the globally averaged age approaches 2-3*by* with isolated relict surfaces dating back to 3-4*by*.

Global Crater Production Curves: The cumulative power-law function for the global cratering record on Venus exhibits a segment that resembles, at first glance, a crater production curve (1). Consequently, initial studies often assume that a direct comparison can be made, after adjustments for flux and scaling differences. The statistically significant portion of the global cratering curve, however, represents a very narrow window (factor of two in size from 50km to 100km) limited at small sizes by atmospheric shielding effects and loss processes. Uncertain regional geologic histories (2), visible effects of enhanced crater enlargement for craters larger than 100km (3), and statistical uncertainty of small numbers lessen the confidence at large sizes. This narrow range of diameters may yield a production-like slope, but its slope may have little significance. The Apollo 17 site on the Moon also exhibited a production-like slope and indicated that this site would provide some of the youngest basalt samples (4), yet the returned sample ages were among the oldest (5). Enhanced degradation of small craters in a thick particulate surface layer and an insufficient counting area at large sizes accounted for this incorrect estimate (6,7). Yet, the correct relative age could have been easily predicted from simple embayment relations with adjacent maria, thereby underscoring the importance of understanding the local geologic context, stratigraphy, and operative processes - - as well as statistical significance.

Although the tangent of the Venus global curve with a lunar calibration curve can yield a minimum average age, such an approach implicitly assumes that the relative impactor flux and crater scaling relations are reasonably well understood. But the dense atmosphere of Venus introduces significant scaling effects by changing the shape (8) and effective density (9) of the impactor and by arresting lateral crater growth (3). Laboratory experiments clearly demonstrate that crater diameter is largely controlled by impactor size, while at a given velocity depth can be controlled somewhat independently by impactor density for a given target (9). If no other processes operate, an aerodynamically flattened impactor (8) will increase crater diameter for a given mass striking a gravity-controlled particulate target, whereas an aerodynamically streamlined impactor (3,10) will decrease crater diameter. In natural materials with strength, however, gravity-controlled growth requires shock-preconditioning the target into a near-strengthless medium. If impactor velocity has been reduced significantly (6km/s), gravity scaling laws become inappropriate.

Laboratory experiments also reveal that a dense atmosphere introduces both static and dynamic pressure effects (3,11). Even though the total excavated crater mass greatly exceeds the displaced atmospheric mass, crater ejecta leave the cavity within a relatively thin wall (i.e., curtain), thereby substantially decreasing the mass per unit area at any given time (3). At laboratory scales, dynamic pressure effects can reduce cratering efficiency by an order of magnitude (3). Dynamic forces acting to retard outward advance of the base of the curtain are transmitted hydrostatically to the cratering flow field. This can be illustrated experimentally by using a plate positioned just above the surface with a hole to allow passage of the impactor. Ejecta striking the plate spray outwards without returning to the cavity, but interactions with the plate reduce cratering efficiency similar to observed atmospheric effects. Because craters grow non-proportionally (i.e., continuously changes shape by first growing downward, then outward), atmospheric dynamic pressure prematurely arrests lateral growth as shown in Figure 1. The process of arrested lateral growth can be modeled analytically as a cylinder expanding with a constant velocity and constant thickness (3) or numerically using variable thickness and decreasing velocity once subsonic (12), both approaches being consistent with experimental results. Scaling to Venus can be justified since outward crater growth is subsonic for most of the latter stages of crater growth and since atmospheric blast effects appear to be offset from crater excavation (3). This approach reveals that excavation craters on Venus could be reduced by as much as a factor of two. This process is consistent with observations of more pronounced rim heights and greater depths than expected(1,13), particularly once empirically adjusted for gravity (14). If correct, the minimum average age from the global crater inventory approaches 2-3 *by*, in contrast with previous estimates of 0.5-1.5*by* (1).

Crater Preservation States: Craters on Venus seem to be in remarkably similar states of preservation (1). This observation has been used to argue that catastrophic global resurfacing has reset the cratering chronometer(15) or that the surface preserves a record of catastrophic bombardment (16). But similar preservation states of radar-bright ejecta facies may not indicate a common maximum age but resistance to weathering and or very weak erosional processes in order to produce the obvious range of expected morphologies found on the other planets.

Searching for Ancient Venus. Peter H. Schultz

The formation of an impact crater in an atmosphere must generate an intense atmospheric response due to the outward kinematic interactions with the ejecta curtain and containment of the vapor cloud (3,11). As a result, emplacement of the inner ejecta will be accompanied by intense winds and vortices with velocities (100m/s - 400m/s) sufficient to winnow and entrain smaller (<meter scale) ejecta, leaving behind a blocky lag surface for the inner facies and creating turbidite-like, run-out flow of smaller (radar-dark) materials. If winds are the primary erosional agent on Venus, then the inner facies will be archived unless winds of comparable magnitude occur again while the outer deposits provide Venus with a local reservoir of particulates

Impact-generated wind storms may represent one of the principal erosional agents on Venus. Such storms can be inferred from laboratory experiments and from the geologic record (3,17). For example, radar-bright and -dark wind streaks associated with the crater Carson are interpreted as the consequence of upper level winds deflected by the expanding, impact-generated, vapor cloud (3). Equally important, however, is the radar-bright, lineated zone extending westward from Carson and eroding ejecta and run-out flow deposits of the crater Aglaonice (600km away from Carson). This scour zone is interpreted as the trail of the late-stage thermal disturbance initially created by Carson but subsequently dragged westward by the strong winds aloft. Other craters with a wide range of preserved facies exhibit evidence for similar impact-generated windstorms (3,17). The widespread occurrence of other wind streaks could represent more gentle, less intense circulation patterns (18,19) or the final stages of impact-generated disturbances far from the source. Conversely, the absence of similar effects around all craters underscores a true continuum of degradational states, in contrast with the perception of a catastrophic flux.

Identifying Ancient Terrains: Relict ancient terrains on Venus should be characterized by the following features: spatial clustering of relatively large craters with different impact trajectories in a common geologic/tectonic setting; evidence for a wide range of preservation states of the outer radar-dark facies; mantling of crater interiors by radar-dark materials; and occurrence in a radar-dark regional setting. The last characteristic should result from the long-term accumulation of smaller size impact debris and accretion of failed entries (estimated to contribute about 1-10m over the last 3*by*), and perhaps pyroclastics. The general absence or poorly expressed craterless, radar-bright blast haloes (indicative of a thinly veneered regolith) should be another consequence of this long-term depositional history. With these criteria, the "Crater Farm" and a region near Atla Regio are proposed to represent islands in time dating back to at least 3*by*. These regions are intermediate in elevations (i.e., have not been low-lying depositional traps) and are notably deficient in volcanic centers (20,21). The dramatic contrast between this surface and our perception of ancient terrains from other planets simply reflects the long-lived atmospheric shield on Venus, her depositional (rather than erosional) history of its ancient surfaces, and perhaps the relative inefficiency of cratering under the dense atmosphere.

1. Phillips, R.J. *et al.* (1991) *Science* 252, 288-296. 2. Saunders, R.J. *et al.* (1991) Science 252, 249-251. 3. Schultz, Ph.H. (1992) *J. Geophys. Res. 97*, E10, 16, 183-16, 248. 4. Scott, D.H. *et al.* (1972) *U.S. G. S. Misc. Geol. Inv. Map*, I-800. 5. Taylor, S.R. (1982) *Planetary Science: A Lunar Perspective*, Lunar and Planet. Sci. Institute. 6. Lucchitta, B.K. and Sanchez, A.G. (1975) *Proc. Lunar. Planet. Sci. 6th*, 2427-2441. 7. Schultz, Ph.H. *et al.* (1977) *Proc. Lunar Planet. Sci. 8th*, 3539-3564. 8. Melosh, H.J. (1981) *In Multi-Ring Basins*, pp. 29-35, Pergamon, New York. 9. Schultz, P.H. and Gault, D.E. (1985) *J. Geophys. Res. 90*, 3701-3732. 10. Ivanov, B.A. *et al.* (1992) *J. Geophys. Res. 92*, No. E10, 16,167-16,181. 11. Schultz, P.H. (1992) *J. Geophys. Res. 97*, 975,1006. 12. Schultz, P.H. (1990) *Int. J. Impact. Engin* (in press). 13. Basilevsky, S. and Ivanov, B.A. (1990) *Geophys. Res. Letts.*, 175-178 14. Herrick, R. (1992) Analysis of the Impact Cratering Record on Venus (PhD Thesis), Southern Methodist University, Dallas. 15. Schaber, G.G. *et al.* (1992) *J. Geophys. Res. 97*, E8, 13,257-13,301. 16. Bills, B. (1992) Lunar and Planet. Sci. XXIII, 99-100. 17. Schultz, P.H. (1992) *Int. Colloq. in Venus*, LPI Contrib. No. 789, 104-106. 18. Arvidson, R. *et al.* (1991) *Science 252*, 270-275. 19. Greeley R., *et al.* (1992) *J. Geophys. Res. 92*, 13,319-13,346. 20. Crumpler, L. *et al.* (1992) *Int. Colloq. in Venus*, LPI Tech. Contrib. 789, p. 25. 21. Head, J.W. *et al.* (1992) *J. Geophys. Res. 97*, No.E8, 13, 153-13, 197.

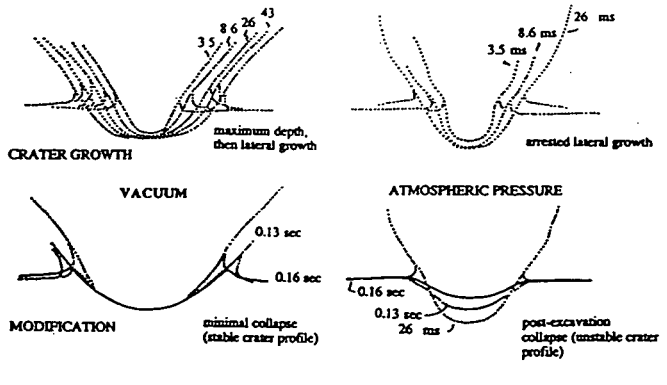

Fig. 1. Atmospheric effects on crater growth from quarter space laboratory impact experiments. Atmosphere retards outward growth of curtain because it behaves as an impermeable plate. Craters in non-cohesive sand form a deep bowl-shaped transient cavity resembling an early stage of growth in a vacuum (left). The transient profile collapses in sand (bottom right) but is preserved in compacted pumice (3,17).

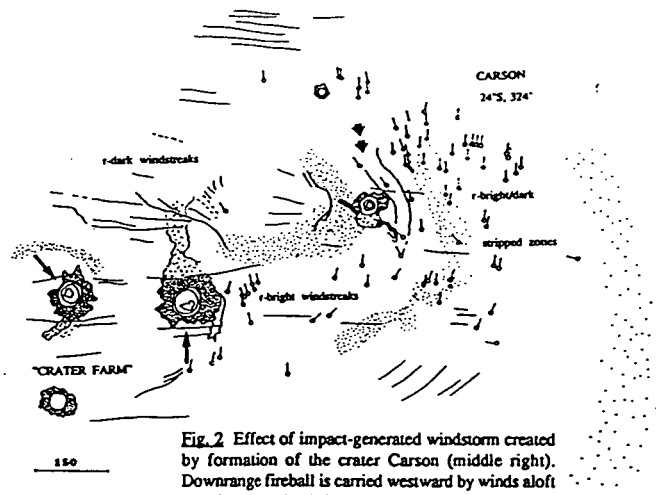

Fig. 2 Effect of impact-generated windstorm created by formation of the crater Carson (middle right). Downrange fireball is carried westward by winds aloft creating a radar-brightened surface (stipple) and scouring ejecta deposits of Aglaonice. Radar-bright winds streaks, scour zones, and radar-dark streaks represent superposition of gradually decreasing winds through time. Different impact directions (arrows) and angles indicate separate impact events. This area is proposed to be an ancient relict of Venus.

Dynamical Evolution of Vapor Clouds by Oblique Impacts on Venus.

Seiji Sugita and Peter H. Schultz, Brown University, Providence RI 02912

Previous studies [1, 2] showed that an oblique impact generates a ballistic vapor cloud that moves downrange and is physically decoupled from the late excavation stage of cratering. The initial downrange translational motion is strongly controlled by the impact angle, whereby lower impact angles (measured from horizon) result in a higher downrange velocity. This study theoretically describes the dynamics of such impact vapor clouds on Venus in order to assess their possible signatures in the geologic record.

Hydrodynamic Calculations: We have constructed a two-dimensional hydrocode based on CIP (Cubic Interpolated Pseudoparticle) method, which has been successfully applied to various kinds of hydrodynamic problems [3]. The initial vapor cloud is assumed to have a circular shape with a radius of 1 km, density of 3 g/cc, internal energy of 28 MJ/kg, and initial downrange translational velocity of 5 or 8 km/s. The initial internal energy corresponds to a 1km-radius object impacting the surface of Venus at 18 km/s and partitioning 25% of the initial kinetic energy into vaporization (including 12 MJ/kg for the phase transition). The ambient Venus atmosphere is assumed to be an ideal CO_2 gas with temperature of 740°K and pressure of 92 bar. Planar symmetry is also assumed. In these initial calculations, we excluded the effect of the atmospheric density decrease with altitude as well as the effect of radiation and ionization, which would decrease the expansion rate of the vapor clouds. Radiation would accelerate cooling, while ionization would absorb a significant amount of internal energy, which is expressed as reduced kinetic energy in the cloud. Thus the effective cross section of our vapor cloud is over estimated, resulting in an underestimate of the downrange travel distance.

The dynamical response of a vapor cloud moving downrange at either 5 km/s or 8 km/s in the dense atmosphere of Venus is similar. First, highly compressed impact vapor expanding against the ambient atmosphere creates a strong shock front (Fig 1a). Because the translational velocity of the vapor, atmospheric response is asymmetric: elongated in the direction of the translational motion with higher pressure at the leading front and lower pressure at the tail (Fig. 1b). As the shock front develops, expansion decreases the density, pressure, and temperature of the inner core, thereby producing a shell-like structure (Fig. 1c). The downrange motion enhances density and pressure at the leading front and results in a hemispherical shell. As this shell travels farther downrange, Rayleigh-Taylor (R-T) instability develops on the leading front and Kelvin-Helmholtz instability is produced on the sides (Fig. 1d). The R-T instability evolves into plumes associated with vortices (Fig. 1e). By this time, temperature in the impact vapor cloud has decreased close to the condensation temperatures for silicate and metals (3,000 - 4,000°K). Due to the absence of radiational cooling, however, this temperature is overestimated here. The downrange motion of the vapor cloud also has stopped by this time with the total downrange travel distance for the center of mass achieving 9 or 23 times of radius of the initial vapor cloud for the cases of 5 km/s or 8 km/s initial downrange velocity, respectively. It should be noted that the 60% increase in initial downrange velocity results in a 155% increase in total travel distance. Presumably this results from dynamic reshaping of a vapor cloud. The shape of shock front in Fig. 1d evolves into an elongate (rather than hemispherical) front, which reduces the effective cross section of the vapor cloud. The reshaping is more pronounced in the higher downrange velocity case and results from greater shock pressure (hence larger propagation velocities) at the leading front. This dynamical reshaping may be similar to the shock collimation effect previously observed experimentally [1, 4].

Runout Flows around Venus Craters: Runout flows from craters on Venus occur downrange and appear to be deposited prior to lobate ejecta for sufficiently low-angle impacts as determined by the distribution of ejecta [1]. These observations suggest that the runout flows may have evolved from melt and condensation of impact vapor. The runout flows appear to have a "source region" that becomes more offset from the crater center with decreasing impact angle. The runout flow source region is identified as an area where runout flows change their flow direction from impact-controlled (i.e., downrange) direction to gravity-controlled (i.e., topographic gradient) direction. We use the uprange edge of this central structure (i.e., central peak or central peak ring) as a first-order approximation for the point of maximum energy transfer, which is offset from the geometric center and depends on the impact angle [1, 5]. As impact angle decreases, this region shifts uprange relative to crater center. Downrange offset (L) of runout flow source regions is scaled by impactor radius (r_p) for comparison with theoretical results. Impactor radii are estimated from scaling relations based on the size of central structures of craters [6]. Although impactor size also can be estimated from scaling relations for the pre-collapsed crater size [7], the scaling relation based on central structure diameters significantly reduces scatter in the data in Fig. 2. Impact angle is estimated from the uprange ejecta missing sector angle [1, 8]. Downrange offset of runout flow source regions has a very strong and clear anti-correlation with impact angle (Fig. 2). This indicates that a larger fraction of the initial momentum of an impactor is inherited by the vapor cloud as impact angle decreases [1]. If we apply our initial results to these observations, L/r_p values of 8-30 for 40° impacts on Venus would correspond to about 5-10 km/s for the initial downrange translational velocity of a vapor cloud.

DYNAMICS OF IMPACT VAPOR CLOUDS ON VENUS: S. Sugita and P.H. Schultz

A distinctive morphologic feature of runout flows on Venus is their branching into separate lobes [1]. Although branching far from the runout flow source regions are probably a local topographic effect, some branching develops very close to crater rims and appears to be independent of local topography. Some of the proximal branchings may result from R-T instabilities observed in our theoretical study as well as disruption of the impactor.

References [1] Schultz, P.H. (1992) *JGR*, **97**, 16183-16248, [2] Sugita, S and P.H. Schultz (1994) *LPSC abstract* **25** 1355-1356, [3] e.g., Yabe, T. *et al.* (1994) *J. Geomag. Geoelectr.* **46**, 657-662, [4] Schultz, P.H. and S. Sugita (1994) *LPSC abstract* **25** 1215-1216, [5] Schultz, P.H. (1994) *LPSC abstract*, **25**, 1211-1212, [6] Schultz, P.H. and D.E. Gault (1993) *LPSC abstract*, **24**, 1257-1288, [7] Schmidt, R.M. and K.R. Housen (1987) *Int. Impact Eng.* **5**, 543-567, [8] Gault, D.E. and J.A. Wedekind (1978) *Proc. Lunar Planet. Sci. Conf. 9th*, 3843-3875

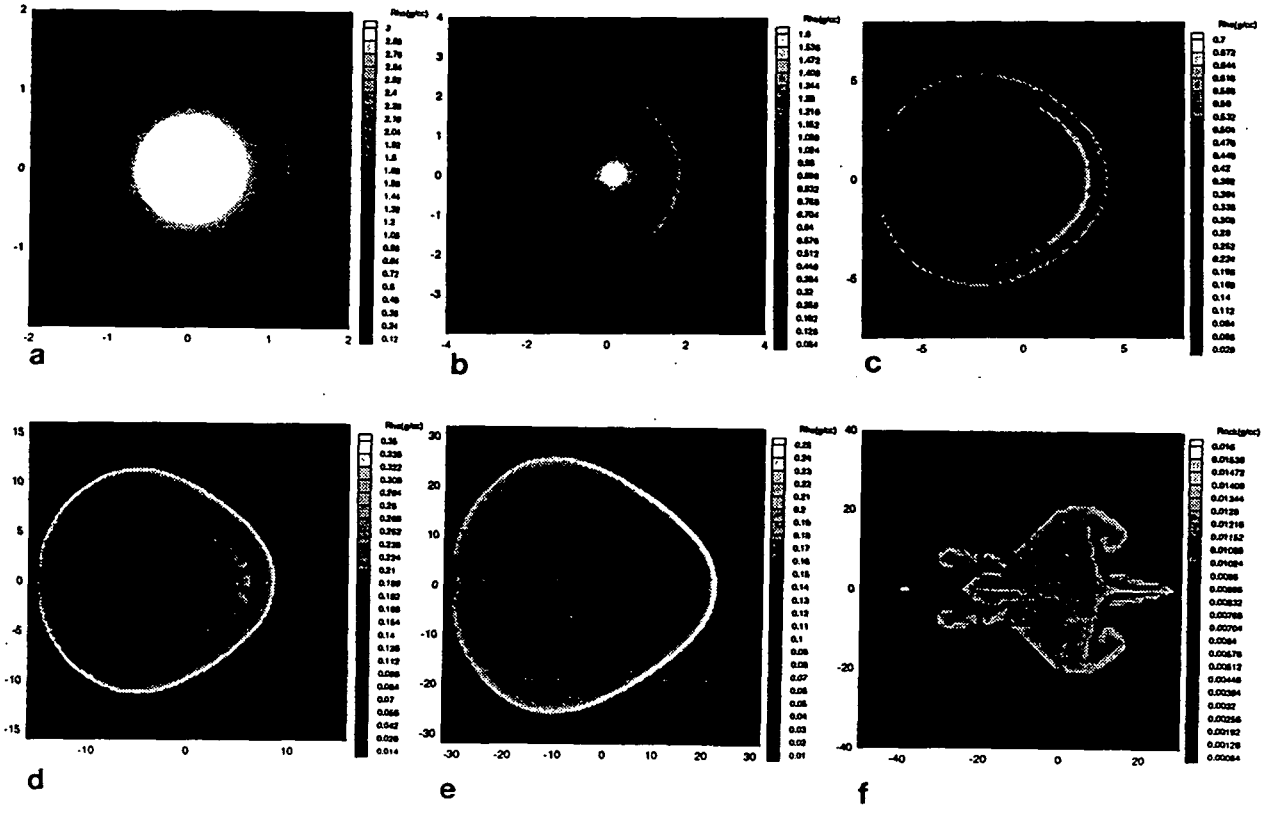

Fig. 1 Time sequence of density distribution of a vapor cloud on Venus. Impact direction is from left to right. The center of mass of impact vapor is fixed at the origin in each diagram. The axis scale is in kilometer. Time after impact and downrange travel distance for each frame are; a) 0.08s, 0.63km, b) 0.28s, 2.2km, c) 0.77s, 5.2km, d) 2.3s, 11.1km, e) 9.9s, 19.8km, f) 44.5s, 23.1km, respectively. The diagram (f) shows density only within the impact vapor cloud.

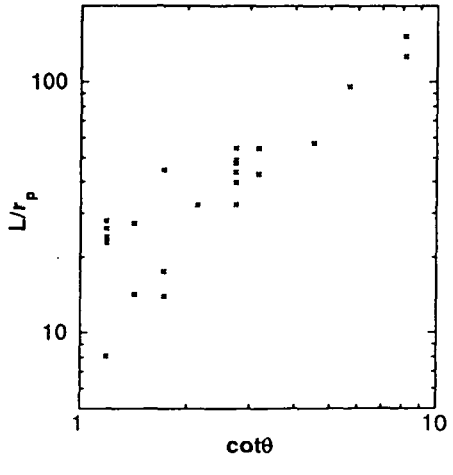

Fig. 2 Observed downrange offset of the runout flow source region as a function of impact angle, θ, for craters on Venus. The downrange offset, L, is scaled by impactor radius, r_p, and is measured from the position of the central peak. Such observations allow estimating the initial translational velocity of the vapor cloud through comparisons with theoretical results as discussed in the text.

Islands in Time on Venus

P.H. Schultz (Department of Geological Sciences, Brown University, Providence, RI, 02912, 401-863-2417, Peter_Schultz@brown.edu)

The globally averaged surface age of Venus is widely considered to be about 0.5 by. Younger or older surfaces over smaller regional areas, however, are difficult to assess due to atmospheric filtering of smaller impactors globally and geologic resurfacing regionally. Various models of the Venus interior are emerging to account for the perception that all craters are well preserved, that few have been volcanically and tectonically modified, and that it is difficult to distinguish the cratering record from a non-random impact record. Although craters generally appear to be in a similar state of preservation, such a perception is based on preservation of coarse inner ejecta deposits that are largely insensitive to physical weathering processes. A full range of preservation states of the more sensitive outer ejecta facies can be documented. The pristine appearance of craters is suggested to reflect a combination of low eosion rates and processes associated with crater formation in a dense atmosphere rather than a youthful epoch of formation. The apparent absence of a large number of volcanically embayed craters is difficult to assess because of our planetary template. On the Moon, impact craters are removed both by embayment and by self-destruction due to crater-controlled volcanism over a relatively limited time (1 by). On Venus, the paucity of volcanically buried craters could reflect globally sustained activity on a regional scale at different times. Craters within active zones would be expected to be totally consumed similar to the interior lunar maria. Lastly, estimates for the global time scale are based on the incorrect assumption that a global crater production function exists. The filtering of crater-producing impactors at small scales, the global paucity of larger craters, regional concentrations of medium-size craters, and the possible effects of atmospheric containment of crater growth lead to the conclusion that the surface actually dates back to 2-3 by globally and perhaps 3-4 by locally. The oldest surfaces generally occur in regions bounded by fracture belts, ridge/mountain belts and shield fields. Such islands in time may represent cores of crust that statistically avoided destruction or perhaps were tectonically shielded within larger impact basin scars dating back to the end of heavy bombardment.

1. 1994 Spring Meeting
2. 00091735
3. (a) P.H. Schultz
Dept. of Geo. Sci.
Box 1846
Brown University
Providence, RI 02912
(b) Phone: 401-863-2417
(c) Fax: 401-863-3978
4. P
5. (a) P01 Is Venus Past its Prime?
(b) 5415, 5455, 5470
6. Oral
7. 20%
8. $50 Check enclosed
9. I (by Session Chair James W. Head, III)
10.
11. No

Penetrating and Escaping the Atmospheres of Venus and Earth. Peter H. Schultz and Seiji Sugita, Department of Geological Sciences, Brown University, Providence, RI 02912.

The smallest single crater on Venus is only about 2 km in diameter (1), even though various models suggest that much larger objects should disrupt, decelerate, and disperse (2). Moreover, inversion of Tunguska-like blast limit dimensions indicate that the largest objects failing to reach the surface without catastrophic failure approach 4 km (3). The contrast between limiting sizes of "survivors" and "blasters" suggests that atmospheric entry may affect different types of objects differently. An important clue for resolving this paradox can be found in laboratory experiments documenting the dispersal and deceleration of hypervelocity debris clouds during atmospheric entry (3, 4). Such experiments and theoretical considerations reveal that interacting shocks act to collimate (rather than disperse) fragments below a critical size, which depends on the lateral velocity and atmospheric density. Schlieren imaging using the NASA-Ames Vertical Gun reveals that smaller fragments "surf" the inner shock front, and the entire debris cloud reshapes to a needle-shape form, thereby reducing deceleration by minimizing the drag coefficient. These results have significance not only for surviving entry to low altitudes but also for atmospheric escape of high-speed ejecta and siblings following low-angle impacts.

Laboratory Experiments: Hypervelocity debris clouds were produced by passing intact pyrex or aluminum spheres through thin mylar or aluminum sheets, respectively (5). Spall velocities spread the resulting fragments into a cluster that expands with time. Under low atmospheric densities, fragments dispersed due to interacting bow shocks as described in (2); however, under high densities (air at one bar) the fragments became tightly collimated with little deceleration (3, 4). Witness plates placed at various distances along the trajectory document the pattern, but Schlieren imaging allows witnessing the process. Schlieren imaging uses collimated light focused on a knife edge to reveal subtle variations in atmospheric density. A short duration flash freezes the image on film. The large impact chamber and side-viewing ports at the NASA-Ames Vertical Gun are ideal for this approach. Effects of ionization and impact flash preclude use at very high velocities (M~> 10), but comparison of dispersal patterns on witness plates up to M = 20 establish the similarity of the process over a wide range of velocities.

Figure 1a provides reference for the shock pattern around a single projectile just before impact under 1 bar atmospheric pressure (air). Figure 1b reveals the separate mach cones around individual fragments under an atmosphere pressure of 0.125 bars. Because schlieren imaging projects three dimensions onto a two-dimensional plane, overlapping mach cones do not necessarily represent interactions. Figure 1b reveals the effect of differential drag acting on different size fragments with larger mach angles documenting lower velocities. At one bar pressure (air), however, individual fragments are contained within a mach cone generated by a leading cluster (Fig. 1c). Differential pressure along the gradient within the boundary shock force individual fragments inwards toward the lower density wake, i.e., they "surf" the mach cone.

Witness plates demonstrate that the same process occurs at M = 18 while high-frame rate photography reveals that the leading front of the debris cloud undergoes little deceleration over the 2 m path length (see 5). Different combinations of ambient pressures, densities, and sound speeds (e.g., use of a helium atmosphere) reveal that the dispersal pattern of the projectile during disruption is not affected by the pressure differential at the break-up diaphragm situated between the evacuated launch tube and impact chamber.

Collimation within a mach cone also occurs for high-speed ejecta and ricochet debris after impact. Such a process was previously inferred from the contradiction between theory and experiments (6). Theory predicted that drag deceleration should prevent sufficiently small ejecta from escaping the cavity, whereas experiments demonstrated that this process was defeated by ballistic shadowing. Schlieren imaging documents this process (Fig. 2). Again a key requirement is that lateral dispersion velocity is small relative to the translational velocity.

Modeling the Process: Containment by the mach surface can be modeled by balancing forces along the pressure gradient across the shock front. Figure 3 illustrates the results for three different planetary environments using the ambient surface pressure for reference. A fragment will escape if the outward force (due to its lateral velocity and diameter relative to the bow shock thickness) exceed the pressure barrier created by the shock boundary, i.e., below the relevant curve. Conditions leading to collimation, therefore, depend on the style of failure and fragment size. Catastrophic disruption resulting in numerous small fragments and high dispersion velocities will escape into ambient conditions outside the mach cone (actually a column at hypervelocities). Non-catastrophic disruption or dispersal of a weak brecciated or regolith-covered object should result in collimation. For example, a bow shock thickness of 100 m (10% of the leading mass) will retain smaller fragments provided that the dispersal velocity due to disruption is less than 33 m/s (Mars), 0.44 km/s (Earth), or 4.5 km/s (Venus) if disruption occurs just above the surface. In reality, a weak object will begin to fail at a high altitude during entry (e.g., comparable to Martian surface conditions) and undergo successive failure as it penetrates to lower altitudes. Collimation of smaller fragments reshapes the debris cloud, thereby further reducing drag (i.e., pressure forces and deceleration).

Implications: High-velocity natural objects may be able to penetrate dense atmospheres to greater depths than previously expected if they undergo disruption at altitude before developing large dispersal velocities generated by

high dynamic pressures. This process allows smaller disrupted objects to reach the surface at velocities much higher than allowed simply by deceleration of rigid bodies. When the effective density of the debris cloud approaches the compressed atmospheric density at lower altitudes, however, catastrophic deceleration should occur. Conversely, this process provides a mechanism by which high-speed ejecta can escape a dense atmosphere with minimal deceleration and without the need for wholesale atmospheric blow-off. Ricocheted debris and ejecta streams created by lower angle impacts provide escape routes for subsequent ejecta, perhaps contributing to ray-like patterns of impact glass and tektites on Earth.

(1) Phillips, R.J. *et al.* (1991), *Science, 252*, 288-296. (2) Melosh, H.J. (1981) in *Multi-Ring Basins*, pp. 29-35, Pergamon, NY. (3) Schultz, P.H. (1992), *J. Geophys. Res., 97*, 16,183-16,248. (4) Schultz, P.H. and Gault, D.E. (1992), *Lunar Planet. Sci. XXIII*, 1235-1236. (5) Schultz, P. H. and Gault, D.E. (1985), *J. Geophys. Res., 90*, 3710-3732. (6) Schultz, P.H. and Gault, D.E. (1979), *J. Geophys. Res., 84*, 7669-7687.

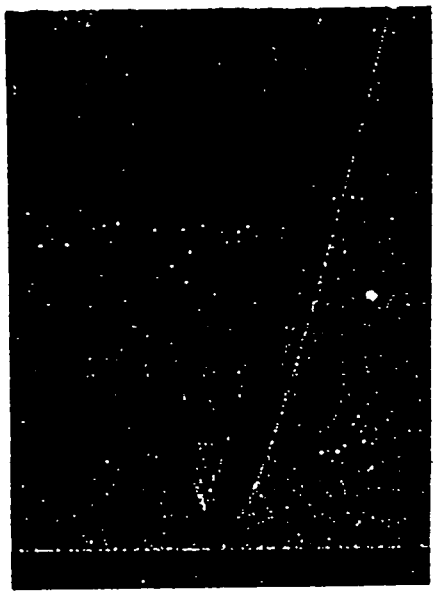

Figure 1a. Mach cone associated with a single 0.635 cm diameter aluminum projectile traversing a 1 bar (air) atmosphere at 1.8 km/s.

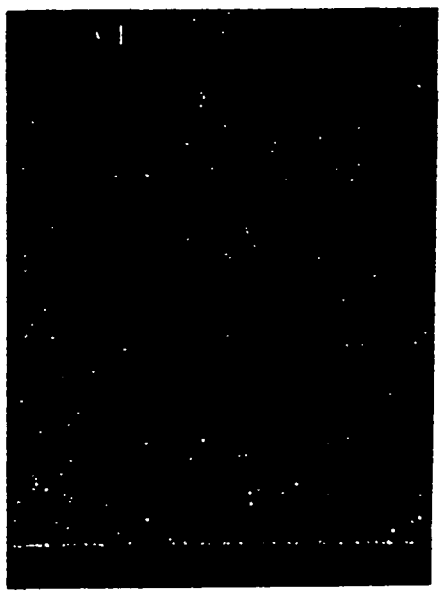

Figure 1b. Separate mach cones associated with larger fragments of a disrupted pyrex sphere traversing a 0.125 bar (air) atmosphere at 1.8 km/s. Fragments spread apart relative to vacuum conditions due to interacting bow shocks; trailing smaller fragments have yet to appear.

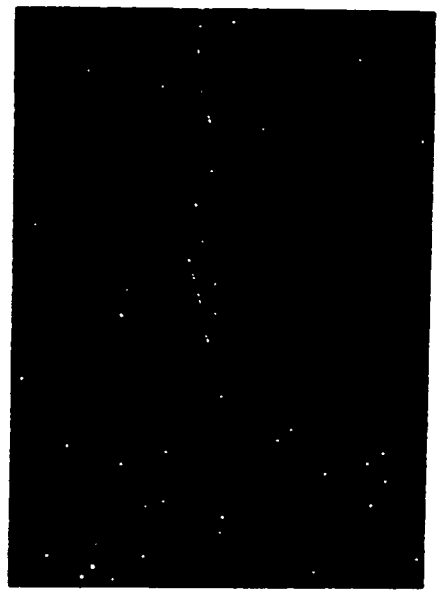

Figure 1c. Collimation of 1.7 km/s impactor fragments within a mach cone created by a group of leading fragments in a 1 bar (air) atmosphere. This process occurs only at higher atmospheric pressures when differential forces created along the shock front exceed the lateral momentum of each fragment. Deceleration of the entire cloud is substantially reduced

Figure 2. Ballistic shadowing created by downrange ejecta from a slightly oblique impact (60°) into a carbonate target at 3.6 km/s under 1 bar (air). Impact point is to lower right; impactor mach surface (only downrange half) extends to right. Vaporization at impact creates downrange "bubble". High-speed ejecta break through the vapor-induced blast downrange within overlapping mach cones

Figure 3. Conditions leading to mach collimation of debris for different planetary environments (for illustration, assumed to be surface pressure). Fragment sizes (scaled to width of shock front) will be contained by the mach cone (mach column for hypervelocity) if the lateral velocity due to breakup falls below the plotted envelope.

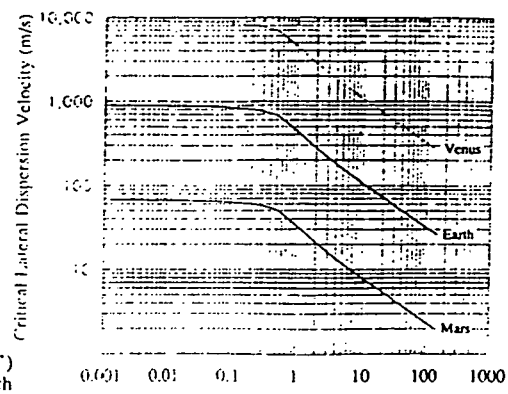

Impact Ejecta Vapor Cloud Interference Around Venus Craters

Seiji Sugita and Peter H. Schultz, Dept. of Geological Sci., Brown Univ. Providence, RI, 02912; e-mail address, sugita@stout.geo.brown.edu

Both experimental and theoretical studies indicate that large scale hypervelocity impacts produce significant amount of impact vapor during cratering [1, 2]. Most of the impact vapor escapes a planet without an atmosphere or with a thin atmosphere [3]; even the terrestrial atmosphere cannot contain vapor cloud [4]. The extremely dense atmosphere of Venus, however, can contain the vapor cloud generated by a lower angle impact [5]. A portion of the impact vapor retains the energy, mass, and translational momentum largely decoupled from later stage vapor/melt generation and excavation of the target. The present study assesses the dimensions of the zone on Venus where the impactor-driven vapor cloud interferes with later ejecta emplacement. The purpose is to derive constraints on the vapor cloud motion including the downrange velocity and expansion velocity.

Impact Vapor Clouds on Venus: Runout flows on Venus indicate an origin initially controlled by the impactors. Runout flows of oblique impact craters occur downrange with some examples climbing up slope before redirected by gravity. Such observations led to the hypothesis that an impact vapor cloud produced by an oblique impact has a large translational downrange momentum [5]. A hemispherical shock formed by the impact vapor explosion expands radially, carrying away the kinetic energy of the vapor cloud. This energy coupling between inner vapor cloud and surrounding air cools the vapor cloud and results in vapor condensation. The vapor condensates contribute runout flows on the surface but represent only a portion of the total energy partitioned to internal energy (impact melt/vapor) of the target. The downrange motion decelerates very quickly due to drag forces. Interference between this early-stage process and later stage ballistic ejection produces an interference zone exhibiting turbulent emplacement styles. This interference zone resembles a parabola open downrange with a shape qualitatively related to impact angle (based on the asymmetry of later stage ejecta deposites).

Observation: Selected craters with well defined ejecta interference zones provide a quantitative measure of the relative effects of lateral expansion and downrange deceleration. Impact angle is estimated by uprange ejecta missing zone according to [5] with an error of ±20%. Projectile size is estimated using both the scaling law for crater diameter [7] including 25% of crater widening and a scaling law based on dimensions of central structure of a crater [8]. But the derived sizes agree very well. Runout distance of a flow is defined as the distance from the uprange edge of the interior structure of the crater (central peak and peak ring) and the point where the flow direction begins to be controlled by topography. The uprange edge of the central structure of the crater is a first-order indicator of first contact point between the impactor and the target [5].

Even though the estimate of impact angle is only approximate, a systematic increase in runout distance relative to width of ejecta interference zone with decreasing impact angle is observed: The ratio of runout distance of the flow to width of ejecta interference zone increases from about 1.1 for relatively high impact angle (~40°) to 1.4 for lower angle (~10°). The ratio for an extremely low angle (<7°) elongate crater approaches 2.5. This supports the hypothesis that the downrange motion of vapor cloud is controlled by an initial momentum inherited from the impactor.

Fluid dynamic Calculation: An analytical fluid dynamical model calculation provides an estimate of the downrange velocity of vapor clouds for the selected craters. The radial expansion of the vapor is described by Taylor's approximation [9]. The shock front expands in proportion to $t^{2/5}$ where t is time. But when shock detaches from the vapor/air interface,

the interface expands with time raised to a power of $2/5\gamma$. This provides the vapor cloud dimensions. The deceleration of translational motion of a vapor cloud is described by

$$m\frac{du}{dt} = -\pi C_D \rho_{air} R^2 u^2 \qquad (1)$$

where m, u, C_D, ρ_{air}, and R are mass, translational velocity, drag coefficient, and radius of the vapor cloud, respectively. Drag coefficient, C_D, depends on shape of the vapor cloud, which is assumed to approximate a sphere with C_D about 0.5 [10]. But if the cloud hydrodynamically reshapes itself, C_D can be much smaller and vary with time [11].

This simple analytical model reproduces the observed quasi-parabolic shape of ejecta interference zone, which becomes more elongate with decreasing impact angle due to a higher initial translational velocity. But absolute values for the derived initial translational vapor cloud velocities required to fit the observed interference zones typically appear to be higher than reasonable values of the impactor velocities. This result possibly indicates that the drag coefficient for the vapor cloud is much smaller due to aerodynamic reshaping during deceleration.

Summary: Dimensions of the ejecta interference zone were measured for a number of selected craters. Runout distances increase as impact angle decreases, but very high initial vapor cloud velocities are derived. These observations are consistent with a vapor cloud has a significant impactor component, which is physically decoupled from later stage excavations for lower angle impacts (<30°). More detailed analyses should allow inverting observations to give better estimates of initial impact conditions.

References: [1] Schultz, P. H. and Gault, D. E. (1990) *GSA Special paper*, **247**, 239-261; [2] O'Keefe, J. D. and T. J. Ahrens (1982) *JGR*, **87**, 6668-6680; [3] Vickery, A. M. (1986) *JGR*, **91**, 14139-14160; [4] Vickery, A. M. and H. J. Melosh (1990) *GSA Special paper*, **247**, 289-300; [5] Schultz, P. H. (1992) *JGR*, **97**, 16183-16248; [6] Sleep, N. H. et. al., *Nature*, **342**, 139-142; [7]Schmidt, R. M. and K. R. Housen (1987) *Int. J. Impact Eng.* **5**, 543-567; [8] Schultz, P. H. (1994) New Development Regarding the K/T Event and Other Catastrophics in Earth History; [9] Taylor, F. R. S.(1950) *Royal Soc. London, Phil. Trans.*, **201**, 159-174; [10] e.g., Shapiro, A. H. (1953) *The dynamics and thermodynamics of compressible fluid flow*, The Ronald Press Com., New York; [11] Schultz, P.H. and S. Sugita (1994) *LPSC* abstract, this volume.

EFFECT OF IMPACT ANGLE ON VAPORIZATION

Peter H. Schultz
Brown University, Department of Geological Sciences
Box 1846, Providence, RI 02912

Submitted to *Journal of Geophysical Research*
(July, 1995)

ABSTRACT

Impacts into easily vaporized targets such as dry ice and carbonates generate a rapidly expanding vapor cloud. Laboratory experiments performed in a tenuous atmosphere, allow deriving the internal energy of this cloud through well established and tested theoretical descriptions. A second set of experiments under near-vacuum conditions provides a second measure of energy as the internal energy converts to kinetic energy of expansion. The resulting data allow deriving the vaporized mass as a function of impact angle and velocity. Although peak shock pressures decrease with decreasing impact angle (referenced to horizontal), the amount of impact-generated vapor is found to increase. Moreover, the temperature of the vapor cloud appears to decrease with decreasing angle. These unexpected results are proposed to reflect the increasing roles of shear heating and downrange hypervelocity ricochet impacts created during oblique impacts.

IMPACT VAPOR GENERATION INFERRED FROM RUN-OUT FLOWS ON VENUS. Seiji Sugita and Peter. H. Schultz; Brown University, Providence, RI 02912

Oblique impact craters on Venus are commonly associated with long run-out flows extending downrange. Parametric hydrocode calculations are used to assess the variables controlling the downrange off-set of the source region of such flows. We find that the impact-angle dependence of the downrange offset of the source region of the run-out flows measured from the point of impact can be readily explained by energy and momentum coupling efficiencies in the downrange impact vapor/melt.

Introduction: Impact vapor clouds strongly affects the environment of Earth [1, 2, 3] and Mars [4], where the atmosphere is very thin. But their direct geologic record is difficult to identify on these planets (but see [5]). The thick Venus atmosphere, however, can decelerate the expansion and translational motion of a downrange-directed vapor cloud [6]. The contained impact vapor is likely to condense and contribute to run-out flows that extends from certain craters [6, 7]. Thus, Venus is a natural large-scale impact laboratory that allows assessing the evolution of impact vapor. To interpret results of these "natural experiments", we compare observations with both numerical calculations and small-scale laboratory experiments.

Hydrodynamical calculations: We conducted series of numerical calculations over a wide range of parameters to understand the general hydrodynamical behavior of impact vapor clouds in the Venus atmosphere. The initial vapor cloud is assumed to be an ideal gas sphere with uniform density (1 - 8 g/cc), specific energy (25 - 100 MJ/kg) and downrange translational velocity (2 - 12 km/s) in the horizontal direction. The ambient Venus atmosphere is assumed to be an ideal CO_2 gas with uniform temperature (740°K) and uniform pressure (3 - 92 bar). Because of the geometric symmetry of the model vapor cloud, our two-dimensional hydrocode [7] was used with an axisymmetric coordinate system.

Fig. 1 shows the terminal temperature of impact vapor clouds for different initial downrange velocities, V_{tr}, and initial specific energies ε_{vap}, and indicates that if the initial specific energy is too large or if initial downrange velocity is too high, impact vapor does not condense. Although our hydrocode does not include radiational cooling, a simple analytical evaluation shows that its effect is too small to significantly affect a kilometer-size vapor cloud in the Venus atmosphere. This suggests that an impact vapor cloud created by a higher velocity impact (as well as volatile-rich impactors [6]) may leave uncondensed suspension flows extending downrange.

Fig. 2 shows the downrange total travel distance, L, of impact vapor clouds scaled by radius, r_p, of impactor. Note that the downrange total travel distance has a super-linear dependence on the initial downrange velocity. This results from dynamic reshaping of the vapor cloud during its downrange course [6]. The results of the parametric study can be summarized in the form of a semi-empirical scaling law:

$$\frac{L}{r_p} = 13\left(\frac{\rho_{air}}{67\mathrm{kg/m^3}}\right)^{\frac{1}{3}}\left(\frac{\rho_{vap}}{3\mathrm{g/cc}}\right)^{0.4}\left(\frac{M_{vap}}{M_{proj}}\right)^{\frac{1}{3}}\left(\frac{\varepsilon_{vap}}{50\mathrm{MJ/kg}}\right)^{-1}\left(\frac{V_{tr}}{10\mathrm{km/s}}\right)^{1.3} \quad (1)$$

where ρ_{air}, ρ_{vap}, M_{vap}, and M_{proj} are ambient air density, the initial density and the mass of impact vapor cloud, and the mass of projectile, respectively This scaling relation can be rewritten in terms of an energy coupling ratio, $\alpha \equiv$ (initial energy of vapor cloud)/(impact energy), momentum coupling ratio, $\beta \equiv$ (momentum of vapor cloud)/(momentum of impactor), and vapor mass ratio, $\psi \equiv M_{vap}/M_{proj}$:

$$\frac{L}{r_p} = 10\left(\frac{\rho_{air}}{67\mathrm{kg/m^3}}\right)^{\frac{1}{3}}\left(\frac{\rho_{vap}}{3\mathrm{g/cc}}\right)^{0.4}\psi^{0.03}\left(\frac{\alpha}{15\%}\right)^{-1}\left(\frac{\beta}{50\%}\right)^{1.3}\left(\frac{V_{im}}{25\mathrm{km/s}}\right)^{-0.7} \quad (2)$$

where V_{im} is impact velocity. Note the very small dependence of the vapor mass ratio, ψ.

IMPACT VAPOR GENERATION ON VENUS: S. Sugita and P. H. Schultz

Venus: The observed downrange offset, L_{obs}, of the source region of run-out flows on Venus is assumed to represent the total travel distance of impact vapor cloud before becoming controlled by gravity [6, 7]. Observations [7] suggest that L_{obs}/r_p is proportional to $\cot^{\xi}\theta$ where θ is impact angle measured from the horizontal and $\xi = 1 \pm 0.3$. Laboratory experiments of oblique impacts [1] also show that the momentum coupling ratio, β, is proportional to $\cot^{\eta}\theta$, where $\eta \geq 0.7$ over a range of impact angle ($7.5° \leq \theta \leq 30°$). To match the observed angle-dependence ($\xi \approx 1$) of the downrange source region off-set on Venus, equation (2) requires that the energy-coupling ratio, α, of impact vapor cloud should be constant or increase with decreasing impact angle. If vaporization in an oblique impact is controlled only by shock heating within a hemispherical high-pressure region as in a near-vertical impact [8, 9], then the amount of internal energy coupled to the resulting vapor cloud should decrease with decreasing impact angle. This expectation is inconsistent with our analyses of run-out flows on Venus. Such a discrepancy may be explained by vaporization enhancement due to either shear heating or sibling impacts by shock decapitation of projectile [10, 11], because these processes are more efficient in lower angle impacts.

References: [1] Schultz, P. H. and Gault, D. E., *GSA Special Paper, 247*, 239-261 (1990) [2] Alvarez, W. et al., *Nature, 269*, 930-935 (1995) [3] Schultz, P. H. and D'Hondt, S., *Nature*, submitted (1996) [4] Melosh, H. J. and A. M. Vickery, *Nature, 338*, 487-489, (1989) [5] Schultz, P. H., *LPSC abstract, 26*, 1039-1040 (1988) [6] Schultz, P. H. *JGR, 97*, 16183-16248 (1992) [7] Sugita, S. and Schultz, P. H., *LPSC abstract, 26*, 1369-1370 (1995) [8] Gault, D. E. and Heitowit, E. D., *Proc. Sixth Hypervelocity Impact Symp., 2*, 419-456 (1963) [9] O'Keefe, J. D. and Ahrens, T. J., *Proc. 8th Lunar Planet. Sci. Conf.*, 3357-3374 (1977) [10] Schultz, P. H., *LPSC abstract, 26*, 1249-1250 (1995) [11] Schultz, P. H., *JGR*, submitted (1996)

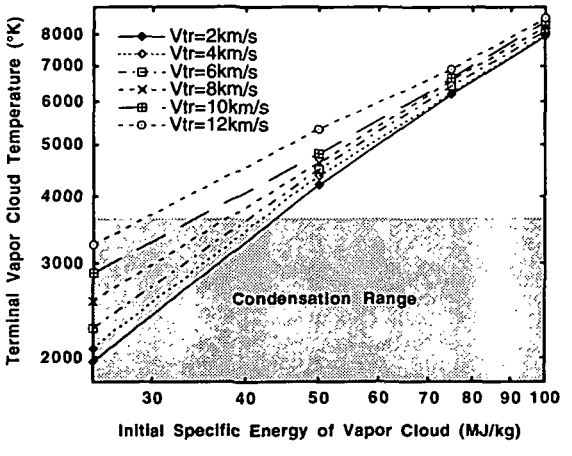

Figure 1. The terminal mean temperature of impact vapor clouds as a function of the initial downrange translational velocity and the initial specific energy of impact vapor clouds, including vaporization energy (12 MJ/kg). The initial density and mass of impact vapor clouds are assumed to be 3 g/cc and equal to projectile mass, respectively. The pressure of the ambient atmosphere is assumed to be 92 bar (Venus surface condition).

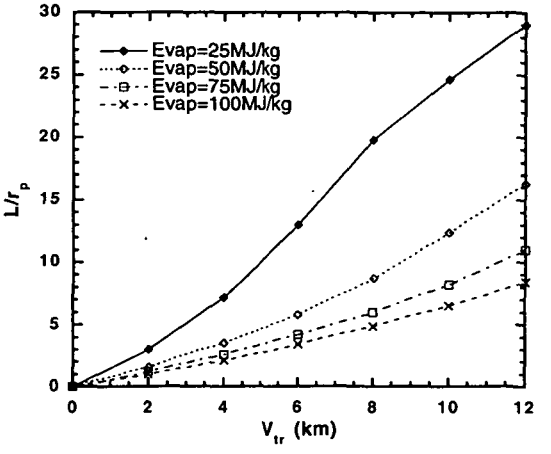

Figure 2. Thé total travel distance, L, of impact vapor clouds scaled by projectile radius, r_p, as a function of the initial downrange translational velocity, V_{tr}, and the specific internal energy, E_{vap}, of impact vapor clouds, including vaporization energy (12 MJ/kg). The calculation parameters are same as in Figure 1.